

On the construction of binary mixture p - x and T - x diagrams from isochoric thermodynamics *

Ian H. Bell and Ulrich K. Deiters

January 2, 2018

Abstract

In this work we describe how to efficiently and reliably calculate p - x and T - x diagrams for binary mixtures of fluids. The method is based on the use of the Helmholtz energy density as the fundamental thermodynamic potential. Through the use of temperature and molar concentrations of the components as the independent variables, differential relationships can be constructed along the phase envelope surface, and this system of differential equations is then integrated to construct isotherms and isobars cutting through the phase envelope.

The use of the Helmholtz energy density as the fundamental potential allows several models to be considered in this formalism, including cubic equations of state (Peng-Robinson, GC-VTPR, etc.) as well as high-accuracy multi-fluid equations of state (the so-called GERG mixture model). Examples of each class are presented, demonstrating the flexibility of this method. Source code, examples, and comprehensive analytic derivatives are provided in the supplemental material.

1 Introduction

The key problem that we are trying to solve is to improve the reliability of phase equilibrium calculations, in particular, the phase equilibrium calculations of binary mixtures, though these techniques and algorithms are directly applicable to multi-component mixtures as well. The “classical” approach to constructing phase envelopes (the locus of points in phase space that separates domains of homogeneous phases from domains where two (or more) phases are in equilibrium) is to carry out many phase equilibrium calculations, taking small increments in a stepping variable while one variable (usually temperature, pressure, or composition), is held constant.

If a reliable starting point for the isoline is available, this algorithm *may* be successful at tracing the entire isoline. On the other hand, there are many reasons why the phase equilibrium calculation may fail at any given point, even if a neighboring point along the phase envelope was successfully calculated:

*Contribution of the National Institute of Standards and Technology, not subject to copyright in the U.S. Commercial equipment, instruments, or materials are identified only in order to adequately specify certain procedures. In no case does such identification imply recommendation or endorsement by the National Institute of Standards and Technology, nor does it imply that the products identified are necessarily the best available for the purpose.

- A density solution (either on the vapor or liquid side) may disappear, and if the algorithm needs to solve for the density as a function of temperature, pressure, and mixture composition, that may not be possible.
- The guesses for the densities and/or compositions of the co-existing phases may not be accurate enough to initialize a derivative-based solver within its radius of convergence.
- There may be a region where the underlying thermodynamic model is not defined or exhibits non-physical behavior (see for instance Bell and Jäger¹).
- The initial guess may be in the critical region, but the solver is not aware of that fact, causing the phase equilibrium calculation to fail in subtle ways.

As demonstrated by Venkatarathnam², many of the supposedly state-of-the-art libraries for tracing phase envelope isolines fail, even for *extremely* simple mixtures. There is a compendium of literature on making phase equilibrium calculations more reliable, but in the end there is no universally reliable algorithm for vapor-liquid equilibrium calculations.

There are existing efforts in the literature to tackle some of the reliability issues with phase envelope construction by constructing lines of constant composition (isopleths) cutting through the phase envelope^{3,4,5}, but there is comparatively less literature on the construction of lines of constant temperature or pressure^{2,6,7,8} around phase envelopes.

This work offers:

- a comprehensive description of how to construct vapor-liquid isotherms and isobars of phase envelopes that ensure thermodynamic consistency.
- analytic derivatives for the complete isochoric thermodynamics formalism for the multi-fluid mixture models of GERG (and other models).
- fully reproducible results through the dissemination of the C++ source code and the Python scripts used to generate each of the figures.

2 Isochoric thermodynamics

The thermodynamic state of a fluid mixture can be uniquely specified by temperature T , molar volume v or density ρ , and a set of mole fractions \vec{x} . This framework of variables is widely used, but has two disadvantages:

- The mole fractions are not independent of each other; if one mole fraction is varied, this affects all other mole fractions.
- Mole fractions are dimensionless properties, while molar volumes or densities have units. Consequently, the $v\vec{x}$ space has no well-defined metric, and this makes it difficult to apply some tools from differential geometry.

There are mathematical solutions or workarounds to these problems, but it is easier to avoid these disadvantages altogether by switching to isochoric thermodynamics^{6,7,9,10,3} —a formulation of thermodynamics that uses molar densities (or concentrations) as its main variables. The central thermodynamic potential of isochoric thermodynamics is the Helmholtz energy density,

$$\Psi \equiv \frac{A}{V} = a\rho, \quad (1)$$

where $\rho = 1/v$ is the molar density of the mixture, V is the total volume and A and a are the total Helmholtz energy and molar Helmholtz energy, respectively. It can be shown^{6,4} that the natural variables of Ψ are the temperature and the molar concentrations

$$\rho_i = x_i\rho, \quad (2)$$

where the vector of molar concentrations is given by $\vec{\rho}$. The molar concentrations ρ_i can be converted to the conventional independent variables of mixture molar density ρ and molar fractions \vec{x} by

$$\rho = \sum_{i=1}^N \rho_i \quad \text{and} \quad x_i = \frac{\rho_i}{\rho}, \quad (3)$$

where N denotes the number of mixture components.

In the formalism of isochoric thermodynamics, the chemical potentials are given by

$$\mu_i = \left(\frac{\partial \Psi}{\partial \rho_i} \right)_{T, \rho_{j \neq i}}, \quad i = 1 \dots N \quad (4)$$

and the pressure by

$$p = -\Psi + \sum_{i=1}^N \rho_i \mu_i. \quad (5)$$

The local curvature of $\Psi(T, \vec{\rho})$ is described by its Hessian matrix, which for a binary mixture is defined as

$$\mathbf{H}_\Psi(T, \vec{\rho}) = \begin{bmatrix} \left(\frac{\partial^2 \Psi}{\partial \rho_1^2} \right)_T & \left(\frac{\partial^2 \Psi}{\partial \rho_1 \partial \rho_2} \right)_T \\ \left(\frac{\partial^2 \Psi}{\partial \rho_2 \partial \rho_1} \right)_T & \left(\frac{\partial^2 \Psi}{\partial \rho_2^2} \right)_T \end{bmatrix} \quad (6)$$

\mathbf{H}_Ψ is a symmetric matrix. For a locally stable state, it must be positive definite, i.e., have positive eigenvalues only. This is a more stringent requirement than the commonly used criterion $\det(\mathbf{H}_\Psi) > 0$, for the latter can be fulfilled if there are two negative eigenvalues, i.e., if the $\Psi(\vec{\rho})$ surface is concave in two directions.

2.1 Deconstruction of Ψ

The molar Helmholtz energy a , and therefore, the Helmholtz energy density Ψ , can be written as the sum of ideal-gas Ψ^0 and residual Ψ^r contributions:

$$\Psi = \Psi^0 + \Psi^r. \quad (7)$$

A universal expression for Ψ^0 is presented in the supplemental material. With Eq. (5) and the discussion in the supplemental material, the pressure can be expressed as

$$p = \rho RT - \Psi^r + \sum_{i=1}^N \rho_i \left(\frac{\partial \Psi^r}{\partial \rho_i} \right)_{T, \rho_{j \neq i}}, \quad (8)$$

where the term ρRT comes from the ideal-gas contribution.

From the subdivision of Ψ , the Hessian matrix of Ψ can then be expressed as the sum of the Hessian matrices of the ideal-gas and residual contributions

$$\mathbf{H}_{\Psi}(T, \vec{\rho}) = \begin{bmatrix} \frac{RT}{\rho_1} & 0 \\ \rho_1 & RT \\ 0 & \rho_2 \end{bmatrix} + \begin{bmatrix} \left(\frac{\partial^2 \Psi^r}{\partial \rho_1^2} \right)_T & \left(\frac{\partial^2 \Psi^r}{\partial \rho_1 \partial \rho_2} \right)_T \\ \left(\frac{\partial^2 \Psi^r}{\partial \rho_2 \partial \rho_1} \right)_T & \left(\frac{\partial^2 \Psi^r}{\partial \rho_2^2} \right)_T \end{bmatrix} \quad (9)$$

where it can be shown (see the supplemental material), that the second partial derivative of Ψ^0 with respect to molar concentration at constant temperature is given by

$$\left(\frac{\partial^2 \Psi^0}{\partial \rho_i \partial \rho_j} \right)_T = \begin{cases} RT/\rho_i & i = j \\ 0 & i \neq j \end{cases} \quad (10)$$

The evaluation of Eq. (9) is much more efficient than Eq. (6) because in the most general case Eq. (6) requires ideal-gas derivatives.

2.2 Isothermal phase equilibrium

The conditions of phase equilibrium at constant temperature can be summarized (again for binary mixtures) as

$$\begin{aligned} \mu'_i &= \mu''_i, \quad i = 1, 2 \\ p' &= p'', \end{aligned} \quad (11)$$

where ' and '' indicate the coexisting phases, liquid and vapor, respectively, in this case. Substitution of Eqs. (4) and (5) gives

$$\left(\frac{\partial\Psi}{\partial\rho_1}\right)'_{T,\rho_2} = \left(\frac{\partial\Psi}{\partial\rho_1}\right)''_{T,\rho_2} \quad (12)$$

$$\left(\frac{\partial\Psi}{\partial\rho_2}\right)'_{T,\rho_1} = \left(\frac{\partial\Psi}{\partial\rho_2}\right)''_{T,\rho_1} \quad (13)$$

$$\Psi'' - \Psi' = \left(\frac{\partial\Psi}{\partial\rho_1}\right)'_{T,\rho_2} \Delta\rho_1 + \left(\frac{\partial\Psi}{\partial\rho_2}\right)'_{T,\rho_1} \Delta\rho_2 \quad (14)$$

Here $\Delta\rho_i \equiv \rho_i'' - \rho_i'$ denotes the concentration difference of component i between the phases. From Gibbs' phase rule, one composition variable can be freely chosen, e.g., ρ_1' .

The conditions of phase equilibrium of Eqs. (12) to (14) can also be expressed directly in terms of residual contributions, where

$$\left(\frac{\partial\Psi^r}{\partial\rho_1}\right)'_{T,\rho_2} + RT \ln \rho_1' = \left(\frac{\partial\Psi^r}{\partial\rho_1}\right)''_{T,\rho_2} + RT \ln \rho_1'' \quad (15)$$

$$\left(\frac{\partial\Psi^r}{\partial\rho_2}\right)'_{T,\rho_1} + RT \ln \rho_2' = \left(\frac{\partial\Psi^r}{\partial\rho_2}\right)''_{T,\rho_1} + RT \ln \rho_2'' \quad (16)$$

$$p' = p'' \quad (17)$$

where p' and p'' are expressed exclusively in terms of residual properties as described in Eq. (8). The isothermal equality of chemical potentials can be converted to the residual form in Eq. (15) and Eq. (16) according to the analysis described in the supplemental material.

Equations (15) to (17) form a system of three nonlinear equations for ρ_2' , ρ_1'' , and ρ_2'' , which can be solved very efficiently by means of the Levenberg–Marquardt method^{11,12} or other numerical methods⁴.

Alternatively, the conditions of isothermal phase equilibrium can be specified as

$$\begin{aligned} d\mu_i' &= d\mu_i'', \quad i = 1, 2 \\ dp' &= dp'' . \end{aligned} \quad (18)$$

This set of equations specifies that the variation of pressure and the chemical potentials along the phase boundary must be the same for both phases. Application of the formalism of isochoric thermodynamics at constant temperature yields the system of first-order differential equations for the molar concentrations in the liquid phase ρ_i' along the phase envelope given by⁷

$$\begin{bmatrix} \mathbf{H}'_{\Psi,1} \cdot \vec{\rho}'' & \mathbf{H}'_{\Psi,2} \cdot \vec{\rho}'' \\ \mathbf{H}'_{\Psi,1} \cdot \vec{\rho}' & \mathbf{H}'_{\Psi,2} \cdot \vec{\rho}' \end{bmatrix} \left(\frac{d\vec{\rho}}{dp}\right)'_{T,\sigma} = \begin{bmatrix} 1 \\ 1 \end{bmatrix}, \quad (19)$$

where $\mathbf{H}_{\Psi,i}$ is the i -th row of the Hessian matrix \mathbf{H}_{Ψ} , and the subscript σ implies that the derivative is taken *along* the phase envelope. The derivatives of the concentrations in the vapor phase can be obtained by solving the system of linear equations given by

$$\mathbf{H}'_{\Psi} \left(\frac{d\vec{\rho}}{dp} \right)''_{T,\sigma} = \mathbf{H}'_{\Psi} \left(\frac{d\vec{\rho}}{dp} \right)'_{T,\sigma}. \quad (20)$$

for $(d\vec{\rho}'/dp)_{T,\sigma}$, where the right-hand-side has already been obtained from Eq. (19). The systems of differential equations given in Eqs. (19) and (20) can be integrated efficiently with adaptive methods like the Cash–Karp algorithm¹³.

We therefore have two complementary ways to compute two-phase equilibria,

- solving a system of nonlinear algebraic equations, Eq. (15) to (17) by means of an appropriate nonlinear system of equations solver. This method requires reasonably good approximations as initial values. Generally, it cannot be guaranteed to converge. If it converges, the precision of the solution does not depend on the quality of the initial values.
- integrating a system of 1st-order ordinary differential equations, Eq. (19) and Eq. (20). This method requires accurate initial values. Convergence is not a problem; the method finds the solutions with certainty as long as the derivatives can be computed with sufficient precision. The precision of the solution at a given location depends on the quality of solutions for previous states.

Both methods do not require the computation of densities from pressure, which can be a time-consuming and problematic step for some equations of state. Moreover, both methods can be extended to multicomponent mixtures.

In some sense, the integration method is analogous to that proposed for the construction of isopleths of phase envelopes through the use of density marching by Venkatarathnam¹⁴; in both methods, the density solver is avoided through the selection of the marching variable to be a density-like variable.

2.3 Isobaric phase equilibrium

When tracing a line of constant pressure of a phase envelope, the same phase equilibria conditions must be fulfilled as for an isotherm: equality of temperature and equality of all chemical potentials between the two phases. According to Deiters⁷, the derivatives of the concentrations in the liquid phase along a phase envelope isobar can be expressed as

$$\begin{bmatrix} \mathbf{H}'_{\Psi,1} \cdot \vec{\rho}'' & \mathbf{H}'_{\Psi,2} \cdot \vec{\rho}'' \\ \mathbf{H}'_{\Psi,1} \cdot \vec{\rho}' & \mathbf{H}'_{\Psi,2} \cdot \vec{\rho}' \end{bmatrix} \left(\frac{d\vec{\rho}}{dT} \right)'_{p,\sigma} = \vec{R} \quad (21)$$

where the right-hand-side column vector \vec{R} is given by

$$\vec{R} = \begin{bmatrix} \left[\left(\frac{\partial \vec{\mu}}{\partial T} \right)''_{\vec{\rho}'} - \left(\frac{\partial \vec{\mu}}{\partial T} \right)'_{\vec{\rho}} \right] \cdot \vec{\rho}'' - \left(\frac{\partial p}{\partial T} \right)''_{\vec{\rho}} \\ - \left(\frac{\partial p}{\partial T} \right)'_{\vec{\rho}} \end{bmatrix}, \quad (22)$$

the derivative of pressure with respect to T at constant molar concentrations (see Eq. (8)) is given by

$$\left(\frac{\partial p}{\partial T}\right)_{\vec{\rho}} = \rho R - \left(\frac{\partial \Psi^r}{\partial T}\right)_{\vec{\rho}} + \sum_{i=1}^N \rho_i \left(\frac{\partial^2 \Psi^r}{\partial T \partial \rho_i}\right)_{\rho_{j \neq i}}. \quad (23)$$

The isothermal difference in chemical potentials $\mu_i'' - \mu_i'$ for the i -th component can be expressed from Eq. (15). Taking a temperature derivative of this difference yields

$$\left(\frac{\partial \mu_i}{\partial T}\right)_{\vec{\rho}}'' - \left(\frac{\partial \mu_i}{\partial T}\right)_{\vec{\rho}}' = \left(\frac{\partial^2 \Psi^r}{\partial T \partial \rho_i}\right)_{\rho_{j \neq i}}'' - \left(\frac{\partial^2 \Psi^r}{\partial T \partial \rho_i}\right)_{\rho_{j \neq i}}' + R \ln \left(\frac{\rho_i''}{\rho_i'}\right) \quad (24)$$

The derivatives of the vapor phase molar concentrations $\vec{\rho}''$ can be obtained by solving the system of linear equations given by

$$\mathbf{H}_{\Psi}'' \left(\frac{d\vec{\rho}}{dT}\right)_{p,\sigma}'' = \mathbf{H}_{\Psi}' \left(\frac{d\vec{\rho}}{dT}\right)_{p,\sigma}' - \left[\left(\frac{\partial \vec{\mu}}{\partial T}\right)_{\vec{\rho}}'' - \left(\frac{\partial \vec{\mu}}{\partial T}\right)_{\vec{\rho}}' \right] \quad (25)$$

Thus Eqs. (21) and (25) allow for the derivatives of the liquid- and vapor-phase equilibrium concentrations at constant pressure with respect to temperature.

3 Mixture modeling

In the formalism presented here, all property evaluations and derivatives are obtained from the Helmholtz energy potential. Many, if not most, thermodynamic models are either already explicit in Helmholtz energy (e.g., SAFT-based models, the GERG multi-fluid mixture model, etc.), or can be converted to a Helmholtz-energy-explicit form (e.g., standard cubic equations of state like van der Waals, Peng-Robinson, Soave-Redlich-Kwong).

In this section, we assume that mixture models can be cast into the framework of the GERG/EOS-CG mixture model^{15,16,17,18}, an empirical mixture modeling approach that combines the highest accuracy pure fluid equations of state with a departure term to correct for deviation from true corresponding states behavior. For more information, the reader is directed to the literature^{17,18}. We further describe how other types of equations of state can be cast into this framework.

The molar Helmholtz energy $a = A/n$ is expressed as a sum of ideal-gas a^0 and residual a^r contributions. Moreover, rather than the molar Helmholtz energy itself, the non-dimensionalized Helmholtz energy $\alpha = a/(RT)$ is used. Rigorously, we actually express the model in terms of the non-dimensionalized Massieu potential $J = -a/T$ (See Span²¹), but for the sake of consistency with existing literature, we will refer to this as a Helmholtz-energy-explicit model formulation.

The Helmholtz-energy-explicit mixture models can be expressed as

$$\alpha(\tau, \delta, \vec{x}) = \frac{a}{RT} = \alpha^0(\tau, \delta, \vec{x}) + \alpha^r(\tau, \delta, \vec{x}), \quad (26)$$

where the independent variables of the Helmholtz energy potential (T, ρ) are expressed instead in terms of the reduced density $\delta = \rho/\rho_r(\vec{x})$ and the reciprocal reduced temperature $\tau = T_r(\vec{x})/T$. The functions $\rho_r(\vec{x})$ and $T_r(\vec{x})$ are reducing

functions that are functions of composition. In some cases (e.g., for cubic equation of state conversions), the reducing functions T_r and ρ_r are actually numerical constants (see for instance Bell and Jäger¹⁹).

The Helmholtz energy density $\Psi = A/V$ expressed in terms of its natural independent variables of τ and δ is therefore given by

$$\Psi = \rho a = \rho \alpha R T = \delta \rho_r R \frac{T_r}{\tau} \alpha(\tau, \delta, \vec{x}). \quad (27)$$

In the methods presented above, it is necessary to obtain first and second partial derivatives of Ψ with respect to molar concentrations at constant temperature, so the task in this section is to express derivatives of Ψ with respect to molar concentrations, but expressing the derivatives themselves in terms of τ , δ , and derivatives thereof.

If we consider Ψ to be a function of τ , δ , and molar composition vector \vec{x} , the total differential of Ψ is therefore given by

$$d\Psi = \left(\frac{\partial \Psi}{\partial \delta} \right)_{\tau, \vec{x}} d\delta + \left(\frac{\partial \Psi}{\partial \tau} \right)_{\delta, \vec{x}} d\tau + \sum_{m=1}^N \left(\frac{\partial \Psi}{\partial x_m} \right)_{\tau, \delta, x_{k \neq m}} dx_m. \quad (28)$$

In this step, all mole fractions are assumed to be independent, as in the GERG monograph¹⁷ and Rowlinson and Swinton²⁰ p. 91. Rigorously, it is not possible for all of the mole fractions to be independent variables ($N - 1$ mole fractions can be independent, and the last one is obtained from one minus the sum of the $N - 1$ mole fractions), therefore the following equations should not be applied to other mixture models.

Alternatively, Ψ can be considered to have the functional dependency $\Psi = f(T, \rho_1, \rho_2, \dots)$ as described above, and thus we can divide Eq. (28) through by $d\rho_i$, yielding the partial derivative of Ψ with respect to a molar concentration with temperature and all other molar concentrations held constant according to

$$\begin{aligned} \left(\frac{\partial \Psi}{\partial \rho_i} \right)_{T, \rho_{j \neq i}} &= \left(\frac{\partial \Psi}{\partial \delta} \right)_{\tau, \vec{x}} \left(\frac{\partial \delta}{\partial \rho_i} \right)_{T, \rho_{j \neq i}} \\ &+ \left(\frac{\partial \Psi}{\partial \tau} \right)_{\delta, \vec{x}} \left(\frac{\partial \tau}{\partial \rho_i} \right)_{T, \rho_{j \neq i}} \\ &+ \sum_{m=1}^N \left(\frac{\partial \Psi}{\partial x_m} \right)_{\tau, \delta, x_{k \neq m}} \left(\frac{\partial x_m}{\partial \rho_i} \right)_{T, \rho_{j \neq i}} \end{aligned} \quad (29)$$

The second derivative of Ψ with respect to ρ_i and ρ_j is constructed from repetitive applications of the product rule to each of the products in Eq. (29), and can be found in Eq. (47) in Table 1. In each of these derivatives, the residual-only Helmholtz energy density Ψ^r may be substituted for the total Helmholtz energy density Ψ .

[Table 1 about here.]

The details of the analytic derivatives required to implement these derivatives are delegated to the supplemental material. Nonetheless, the overarching conclusion is that from the analysis presented in the supplemental material, it is possible to evaluate all the derivatives from analytic derivatives of the mixture model, which removes a number of challenges with numerical derivatives highlighted by Deiters⁷. With these equations, we have expressed the derivatives of Ψ with respect to the concentrations, while expressing each derivative in terms of expressions that can be evaluated from

the GERG/EOS-CG mixture model.

For the algorithm presented in this paper the derivatives of the ideal gas part are not needed in most cases (except, for instance, for calculating the chemical potential). However, for the sake of completeness they are also provided in the supplementary material. The term α^0 can be given by

$$\alpha^0 = \sum_{i=1}^N x_i [\alpha_{o,i}^0(T, \rho) + \ln(x_i)] \quad (30)$$

where $\alpha_{o,i}^0$ is the non-dimensionalized ideal-gas Helmholtz energy of the i -th pure fluid. This term can be evaluated so long as an integrable function for the ideal-gas specific heat is available for each fluid in the mixture. For more information on the pure fluid contributions, see Span²¹. The derivatives of the ideal gas contribution α^0 with respect to the molar concentrations are somewhat involved, complicated by the fact that the independent variables of Eq. (30) are the temperature and the molar density rather than τ and δ .

3.1 Multi-fluid model

The following pure fluids are used in this work as the mixture components, with the reference to the relevant equation of state published in the literature:

- carbon dioxide²²
- ethane²³
- *n*-hexane²⁴
- *n*-octane²⁴
- methane²⁵
- propane²⁶

The binary interaction parameters are all taken from the GERG-2008 model¹⁸.

3.2 Cubic EOS

Cubic equations of state retain an important place in the modeling of mixtures. Deiters⁷ demonstrates how the Peng-Robinson equation of state can be converted to the functional form $\Psi = f(T, \vec{\rho})$ required for the isochoric thermodynamics formalism. Such a transformation is possible for all cubic equations of state; the most common cubic equations of state can generally be written in the form

$$p = \frac{RT}{v - b_m} - \frac{a_m(T)}{(v + \Delta_1 b_m)(v + \Delta_2 b_m)} \quad (31)$$

where Δ_1 and Δ_2 are constants that are set to yield the desired equation of state¹⁹, and a_m and b_m are the mixture attractive term and co-volume. In the work of Bell and Jäger¹⁹, the residual part of the Helmholtz energy obtained from Eq. (31) is expressed in the form $\alpha^r = f(\tau, \delta, \vec{x})$, which is compatible with Eq. (26). The ideal-gas contribution α^0 is obtained from Eq. (30).

In cubic equations of state used with the multi-fluid model, the reducing temperature and density are both constant values (not a function of molar concentration; see Bell and Jäger^{19,1}). As a result, the derivatives of τ and δ with respect to the molar concentration for cubic equations of state are different from those of the multi-fluid models. Therefore, the derivatives (for cubic EOS only) are given by

$$\left(\frac{\partial\tau}{\partial\rho_i}\right)_{T,\rho_{j\neq i}} = 0 \quad (32)$$

$$\left(\frac{\partial^2\tau}{\partial\rho_i\partial\rho_j}\right)_T = 0 \quad (33)$$

$$\left(\frac{\partial\delta}{\partial\rho_i}\right)_{T,\rho_{j\neq i}} = \frac{1}{\rho_r} \left(\frac{\partial\rho}{\partial\rho_i}\right) = \frac{1}{\rho_r} \quad (34)$$

$$\left(\frac{\partial^2\delta}{\partial\rho_i\partial\rho_j}\right)_T = 0 \quad (35)$$

The derivatives of the mole fraction x_m with respect to the molar concentrations ρ_i are unchanged.

3.3 Phenomenology

A vast range of phase equilibria behavior are possible for binary mixtures. For coverage of many of the relevant phase equilibria behavior, see Rowlinson and Swinton²⁰ or Deiters and Kraska⁶.

For cases where the given temperature or pressure value is between the triple-point value and the critical point value of at least one of the pure fluids, it is assured that the phase envelope isotherm or isobar will intersect at least one of the pure-fluid vapor pressure curves. In the case of low-pressure phase equilibrium, this probably (though this is not assured) means that there will be a continuous isoline from one pure fluid to the other.

Throughout this section we shall consider vapor-liquid equilibrium only. The reader should be aware that such equilibria may be metastable at low temperatures with respect to crystallization. Furthermore, some equations of state are valid over a limited temperature range and may be quite inaccurate or create artifacts outside their range of validity.

It is of course crucial that the mixture model is able to properly represent the phase equilibrium behavior of mixtures. Some of the more challenging phase equilibrium behaviors (azeotropy, critical points/lines, double retrograde condensation, etc.) may only appear with a properly tuned mixture model. As a brief demonstration of that, we present in Fig. 1 an isotherm for carbon dioxide + ethane, demonstrating that the conventional Peng-Robinson mixture model (with $k_{ij} = 0$) misses the strength of the positive azeotrope, though it does at least correctly predict the existence of a positive pressure

azeotrope.

The same argument holds for the multi-fluid model. Each binary pair has tuned empirical parameters to best represent experimental datasets. The development of the datasets of empirical parameters has been a multi-decade endeavor among a number of research groups around the world. In recent years, entirely automatic methods have been developed to fit these interaction parameters for many mixtures in parallel²⁷. The emphasis in this work is on algorithms, not representation of experimental data, and we make the assumption that any model employed has already been tuned to well-represent the thermodynamics of the binary mixture.

[Figure 1 about here.]

4 Algorithm

We begin with a discussion of the construction of simple phase equilibrium isolines and progressively increase the complexity of the modeling endeavor.

4.1 “Pure” fluid initialization

While in theory one could begin the integration of the system of differential equations at any point along the phase envelope, starting at a pure fluid endpoint is appealing because the algorithms for phase equilibrium of pure fluids are much more robust than those of mixtures. The primary difficulty for initialization at a pure fluid endpoint is that the ideal-gas contribution to the Helmholtz energy α^0 for pure fluids is undefined because it contains terms of the form $x_i \ln x_i$, which when evaluated at $x_i = 0$, yields $-0 \cdot \infty$. The limit of this product as $x_i \rightarrow 0$ has the value 0. Thus there are three options: a) consider the limiting value when x_i is *small enough*, or b) don’t actually initialize *at the pure fluid*, but very close to the pure fluid, c) derive the analytical limiting value⁷.

In this work, we have decided to initialize the integration at a very small, but nonzero, concentration of the “solute”. In this way, the numerical challenges of infinite dilution, and the discontinuity with very small (but nonzero) concentrations are avoided. This yields a very robust and stable initialization. The initialization very near a pure fluid follows this procedure:

- The pure fluid saturated liquid $\rho'_{o,i}$ and vapor $\rho''_{o,i}$ densities are obtained for the given temperature or pressure, either from a vapor-liquid equilibrium calculation, or from pure-fluid ancillary equations of the form $\rho' = f(T)$, $\rho'' = f(T)$, and $p = f(T)$ if provided. The densities of the coexisting liquid and vapor phases very near the pure fluid should be very near those of the pure “solvent”.
- The molar concentration of the “solute” in the liquid phase ρ'_j is set to a very small value on the order of 1×10^{-6} .
- The molar concentration of the “solvent” in the liquid phase is set to $\rho'_{o,i} - \rho'_j$ (the molar concentrations sum to the total density)

- The molar fractions of the components in the vapor phase are set to the same values as in the liquid phase, which allows the vapor phase molar concentrations to be obtained from

$$\rho_j'' = (\rho_j' / \rho_{o,j}') \cdot \rho_{o,i}'' \quad (36)$$

The term $\rho_j' / \rho_{o,j}'$ is the molar fraction of component j in the liquid phase.

- After the initialization process is complete, vapor-liquid equilibrium is enforced by simultaneously solving Eqs. (15) to (17) and imposing the molar concentration of the solute in the liquid phase according to the isotherm polishing described in the supplemental material.
- A point on the phase envelope has been identified, and the isoline may now be traced.

This initialization methodology brings with it a few challenges: 1) The given temperature/pressure must be between the critical value and the triple-point value for the pure “solvent”. For fluids with short saturation curves (e.g., carbon dioxide), this results in a limited region where near-pure-fluid initialization is possible. For temperatures below the triple-point temperature, initial values could in principle be generated by extrapolating ancillary curves, or other alternatives. 2) This initialization method is not successful for temperatures or pressure that are greater than both of the critical values. It is possible to have an isoline that is detached from both pure fluid endpoints (see for instance Deiters and Kraska⁶) in, for instance, the case of vapor-vapor equilibrium above the critical temperatures of both pure fluids for negative azeotropes. Initialization and marching strategies for supercritical states will be discussed in an upcoming article.

4.2 Marching

The isothermal derivatives given by Eq. (19) and Eq. (20) and the isobaric derivatives given by Eq. (21) and Eq. (25) give three-dimensional derivatives along the phase envelope surface. These derivatives must then be integrated to trace along the contour of the phase envelope. In this framework, we give the marching variable as t and the set of independent variables as the vector \vec{y} . Therefore, the set of differential equations is expressed as

$$\left(\frac{\partial \vec{y}}{\partial t} \right) = f(t, \vec{y}). \quad (37)$$

The marching variable t is selected to take on values from t_{\min} to t_{\max} inclusive.

Integration of the set of differential equations is a rather straightforward process with adaptive step-sizing algorithms, though there are a few details that must be handled carefully:

- As the isoline is traced out, the phase equilibrium conditions of Eqs. (15) to (17) are no longer fulfilled exactly due to integration error. In fact, at each subsequent step (without the “polishing” described below), the pressure and chemical potential of the two equilibrium phases deviate more and more from each other. This will be described further in Fig. 2a.

- In classical adaptive step-size integrators, the allowable error per step is an adjustable parameter specified by the user, and has an impact on both the speed and accuracy of the integration. The smaller the allowable error, the more steps are required, and the less integration error accumulates over the course of the integration. Very small steps also tend to introduce numerical truncation error, so the “best” allowable error per step is a matter of compromise between speed, integration error, and truncation error.
- As the critical line is approached, the set of differential equations becomes extremely stiff; the step sizes required by the integrator monotonically decrease until they reach the minimum step size allowed by the integrator. This is a termination case for the integrator.

4.2.1 Isotherm

Along an isotherm, the differential equations are given by Eq. (19) and Eq. (20). Assuming the initial integration state has been properly initialized, there are two options for marching: 1) pressure is the marching variable and the independent variables are the molar concentrations in both phases 2) one of the molar concentrations is the marching variable and the derivatives of all other concentrations are expressed as a function of the derivative of the first concentration.

In either marching case, at a given evaluation of the derivatives, the temperature and all the molar concentrations are known, and therefore, the derivatives of the concentrations with respect to the pressure at constant temperature along the phase envelope can be evaluated from Eq. (19) and Eq. (20).

Selection of the appropriate marching scheme is described below.

Marching in pressure When pressure is the marching variable, $t = p$, and the vector of independent variables is given by

$$\vec{y} = \begin{bmatrix} \rho'_1 \\ \rho'_2 \\ \rho''_1 \\ \rho''_2 \end{bmatrix}, \quad (38)$$

with the derivatives given by

$$\left(\frac{d\vec{y}}{dp}\right)_{T,\sigma} = \begin{bmatrix} \left(\frac{d\rho_1}{dp}\right)'_{T,\sigma} \\ \left(\frac{d\rho_2}{dp}\right)'_{T,\sigma} \\ \left(\frac{d\rho_1}{dp}\right)''_{T,\sigma} \\ \left(\frac{d\rho_2}{dp}\right)''_{T,\sigma} \end{bmatrix} \quad (39)$$

where the first two terms come from Eq. (19) and the second two from Eq. (20).

The pressure range of integration is set to be from the pressure given from the initialization to a user-specified maximum pressure. In many cases, marching in pressure will result in a traversal of the critical line, which is impossible, and the

integrator will prematurely terminate.

Marching in concentration When marching in the concentration of one component, the marching variable is set to be that of the specified molar concentration $t = \rho'_1$ (here, the molar concentration of the first component in the liquid phase, but any of the concentrations could be selected, resulting in an analogous formulation). The vector of independent variables then becomes the same as in Eq. (38). The vector of derivatives then becomes

$$\left(\frac{d\vec{y}}{d\rho'_1}\right)_{T,\bar{p}',\rho'_{j\neq k}} = \begin{bmatrix} \left(\frac{d\rho_1}{dp}\right)'_{T,\sigma} / \left(\frac{d\rho_1}{dp}\right)'_{T,\sigma} \\ \left(\frac{d\rho_2}{dp}\right)'_{T,\sigma} / \left(\frac{d\rho_1}{dp}\right)'_{T,\sigma} \\ \left(\frac{d\rho_1}{dp}\right)''_{T,\sigma} / \left(\frac{d\rho_1}{dp}\right)'_{T,\sigma} \\ \left(\frac{d\rho_2}{dp}\right)''_{T,\sigma} / \left(\frac{d\rho_1}{dp}\right)'_{T,\sigma} \end{bmatrix}, \quad (40)$$

where the first term is, by inspection, seen to be equal to unity. The liquid-phase derivatives come from Eq. (19) and the vapor-phase derivatives from Eq. (20). In these derivatives, the dp “cancels out”, leaving the desired derivative.

The range of the specified molar concentration is from the near-pure concentration of component two ($\rho'_1 \approx 1 \times 10^{-6}$) to near-pure concentration of the other component ($\rho'_1 \approx \rho'_{o,1}(T) - 1 \times 10^{-6}$). It is not possible to march all the way to the pure liquid composition of the first component $\rho'_{o,1}$ because of the ideal-gas contribution as described in section 4.1; the ideal-gas contribution results in terms of the form $\ln \rho_i$.

4.2.2 Isobar

The derivatives along an isobar are analogous to those along an isotherm, but are more involved because pressure is not one of the independent variables of the Helmholtz energy density. The set of derivatives required for the isobaric case is given by Eq. (21) and Eq. (25).

Marching in temperature When marching in temperature, at a given evaluation of the derivatives, the temperature is known (because it is the marching variable). Therefore, the marching in temperature case is directly comparable to that of marching in pressure for an isotherm. The vector of independent variables then becomes the same as in Eq. (38), and the set of derivatives along the phase envelope is given by

$$\left(\frac{d\vec{y}}{dT}\right)_{p,\sigma} = \begin{bmatrix} \left(\frac{d\rho_1}{dT}\right)'_{p,\sigma} \\ \left(\frac{d\rho_2}{dT}\right)'_{p,\sigma} \\ \left(\frac{d\rho_1}{dT}\right)''_{p,\sigma} \\ \left(\frac{d\rho_2}{dT}\right)''_{p,\sigma} \end{bmatrix} \quad (41)$$

The range of the marching temperature is from the value obtained from the near-pure initialization to a user-specified value. If the specified value is sufficiently high, the isobar may cross the critical line, causing termination of the isoline tracer.

Marching in concentration The most conceptually challenging case to understand is the isobaric case with a molar concentration as the marching variable. In this case, the temperature is one of the independent variables of the integration, and is obtained through integration of its differential equation with respect to the marching variable. The implementation of this integration ends up being not much more complicated than any of the other marching cases.

Here, the marching variable is $t = \rho'_1$ (any of the other concentrations could have been analogously selected), which yields the vector of independent variables given by

$$\vec{y} = \begin{bmatrix} T \\ \rho'_2 \\ \rho''_1 \\ \rho''_2 \end{bmatrix}, \quad (42)$$

with the set of differential equations given by

$$\left(\frac{d\vec{y}}{d\rho'_1} \right)_{p, \bar{p}', \rho'_{j \neq k}} = \begin{bmatrix} 1 / \left(\frac{d\rho_1}{dT} \right)'_{p, \sigma} \\ \left(\frac{d\rho_2}{dT} \right)'_{p, \sigma} / \left(\frac{d\rho_1}{dT} \right)'_{p, \sigma} \\ \left(\frac{d\rho_1}{dT} \right)'_{p, \sigma} / \left(\frac{d\rho_1}{dT} \right)'_{p, \sigma} \\ \left(\frac{d\rho_2}{dT} \right)'_{p, \sigma} / \left(\frac{d\rho_1}{dT} \right)'_{p, \sigma} \end{bmatrix}, \quad (43)$$

where the liquid derivatives come from Eq. (21) and the vapor derivatives come from Eq. (25). The limits of integration for ρ'_1 are the same as described in the concentration marching description in section 4.2.1.

4.3 Refining the solution

As described above, the differential equations along the phase envelope are derived from the iso- p and iso- μ_i conditions specified in Eqs. (15) to (17). These conditions are the *definition* of phase equilibrium for a binary mixture. As the adaptive step size integrator traces out the isoline, error builds up, causing deviation from the equalities of Eqs. (15) to (17). As an initial demonstration of the problem, we present in Fig. 2a the residues for a naïve treatment - the integrator is run, and no polishing of the solution is done as the integration proceeds. Near the end of the integration, the error in pressure is more than 10% for a very liberal allowable error per step of 0.001 (though the last point is not shown in the figure). The solver is not able to get all the way to a unity mole fraction because the last step takes the densities beyond

the pure fluid; a more conservative allowable error would fix this problem. As the allowable error per step is reduced by a few orders of magnitude, the deviations between the liquid and vapor phases also decrease, but are still not negligible.

[Figure 2 about here.]

The deviations as the integration progresses demonstrate that active methods are required to enforce Eqs. (15) to (17) during the course of the integration. The approach taken here is to solve Eqs. (15) to (17) with a conventional Newton-Raphson-based nonlinear system of equations solver. While in principle one cannot guarantee that the Newton-Raphson solver will safely converge, in this case we are never far from the correct solution. Therefore, the Newton-Raphson solver is only doing a small polishing of the solution, and the initial guesses are excellent. Furthermore, we can construct the Jacobian matrix analytically, adding to the reliability of the method as no numerical derivatives are required. Additional checks are applied on the polished solution - for instance that the step taken by the polisher is not *too* large, that the pressure is positive, etc. If the polishing fails (most commonly in the critical region), the unpolished solution is kept.

The Newton-Raphson polisher is given by

$$\mathbf{J} \cdot \Delta \vec{v} = -\vec{r} \quad (44)$$

where \vec{v} is the vector of variables to be polished, \vec{r} is the vector of residues, and \mathbf{J} is the Jacobian matrix. The solution for \vec{v} is updated from $\vec{v}_{\text{new}} = \vec{v}_{\text{old}} + \Delta \vec{v}$ until convergence is achieved.

In the case of the isotherm tracer, the vector of variables to be polished is $\vec{v} = [\rho'_1 \quad \rho'_2 \quad \rho''_1 \quad \rho''_2]^T$, and the vector of residues \vec{r} is given by

$$\vec{r} = \begin{bmatrix} \left(\frac{\partial \Psi^r}{\partial \rho_1} \right)'_{T, \rho_2} + RT \ln \rho'_1 - \left(\frac{\partial \Psi^r}{\partial \rho_1} \right)''_{T, \rho_2} - RT \ln \rho''_1 \\ \left(\frac{\partial \Psi^r}{\partial \rho_2} \right)'_{T, \rho_1} + RT \ln \rho'_2 - \left(\frac{\partial \Psi^r}{\partial \rho_2} \right)''_{T, \rho_1} - RT \ln \rho''_2 \\ p' - p'' \\ \rho'_1 - \rho'_{1, \text{spec}} \end{bmatrix}, \quad (45)$$

where the pressures come from Eq. (8). The Jacobian matrix \mathbf{J} is given in the supplemental material. The approach for the isobaric case is analogous, and is described in the supplemental material.

Figure 2b presents the deviation plots along the same isotherm when polishing of the solution is carried out at every step. These results demonstrate that the Newton-Raphson solver is able to effectively enforce the phase equilibrium conditions, and yield consistent results throughout the integration process. The additional computational overhead of polishing is relatively modest, as is shown below in the computational efficiency results.

4.4 Selecting the marching variable

As described above, we limit ourselves to isolines that can be traced completely (or until their logical termination) by marching in only one variable. This means that for p - x diagrams, either we march in pressure or we march in the molar

concentration of one of the components; for T - x diagrams, we march in temperature or the molar concentration of one of the components. In this work, selection of the marching variable has been carried out in a straightforward fashion:

- For p - x diagrams, along an isotherm, if the temperature is above the minimum of the critical temperatures of the two pure components, pressure is selected as the marching variable, otherwise the molar concentration of one of the fluids is selected as the marching variable.
- For T - x diagrams, along an isobar, if the pressure is above the maximum of the critical pressures of the two pure components, the temperature is selected as the marching variable, otherwise the molar concentration of one of the fluids is selected as the marching variable.

5 Results

5.1 Implementation

The analysis and algorithms described in this work have been implemented in a C++ library available as supplemental material. The algorithm presented here makes heavy use of linear algebra operations, and leverages the open-source C++ linear algebra library `Eigen`. In order to facilitate plotting and the use of this library to carry out calculations, a wrapper of the library was generated for the Python programming language through the use of the `pybind11` package³⁰. Therefore the convenience of a high-level language is retained, while yielding computational efficiency commensurate with the use of a low-level language - the best of both worlds.

Three-dimensional plotting of the phase envelope isolines is carried out as an offline operation. The isolines in temperature and pressure are calculated with the isoline tracing routines and subsequently cached. These isolines are then added together into a three-dimensional object with the open-source `plotlyjs` plotting library through its wrapper for the python language. The library `plotlyjs` generates a standalone HTML file, into which all the javascript required for plotting the isolines is injected. Therefore, a fully-open-source solution can be used to construct the entire three-dimensional phase envelope in a form that can be opened and interactively explored in all modern web browsers supporting the `WebGL` standard.

5.2 Two-dimensional and three-dimensional isolines

Figure 3 demonstrates some of the behavior that can be exhibited by binary mixtures. Figure 3a and Fig. 3b demonstrate p - x and T - x diagrams for n -hexane + n -octane and CO_2 + ethane, respectively. These figures are given in the classical form, with cross-sections of the three-dimensional phase envelope shown for selected values of temperature and pressure. The mixture of n -hexane + n -octane exhibits classical Type I phase equilibrium, with oblong bubble and dew lines that are each monotonic in molar composition. The critical lines for this mixture is continuous and nearly linear in composition between the two pure fluids.

On the other hand, the mixture of CO₂ + ethane demonstrates a positive-pressure azeotrope (at the azeotropic composition, the pressure of the mixture is above that of the pure components at the given isotherm’s temperature)⁶. Along each of the investigated isotherms, so long as the isoline does not intersect the critical line, it has a pressure maximum. This pressure maximum at the azeotrope is traversed without any difficulty. Conversely, along each isobar in the T - x diagram, the isoline tracer must pass through the pressure minimum at the azeotropic composition. Here too, without any difficulty, the pressure minimum is traversed when marching in molar concentration.

The first two systems investigated have relatively simple phase equilibrium behaviors. As we describe below, this algorithm is also well-suited to the calculation of isotherms for which one (or more) of the fluids is supercritical. Figure 3c shows selected supercritical isotherms for a mixture of methane and n -propane. In this case, the Peng-Robinson model with $k_{ij} = 0$ was used because the algorithm of Bell and Jäger¹ was unable to yield a continuous critical line for the multi-fluid model though that of Peng-Robinson succeeded. This figure demonstrates that without any special treatment we can trace all the way up to the critical line. This figure also clearly demonstrates that the critical point of a phase envelope isotherm corresponds to the maximum of the isotherm as described by Deiters and Kraska⁶.

[Figure 3 about here.]

Figure 4 presents the results of Fig. 3b in a three-dimensional form. While the results are fundamentally equivalent, the phase envelope of binary mixtures is rarely, if ever, presented in a three-dimensional manner similar to this figure. Aside from its purely aesthetic value, the three dimensional representation of the phase envelope is very useful from a pedagogical standpoint in educating new chemical engineers about multi-phase equilibria, and the interplay between state variables for multi-phase equilibria.

[Figure 4 about here.]

While the emphasis in this paper thus far has been on “simple” phase envelopes, the techniques developed in this work are particularly well suited to challenging mixtures as well (e.g., those with discontinuous critical lines, open phase envelopes, etc.). Very little *a priori* knowledge is required about the shape of the phase envelope. Tracing steps can begin near the pure fluids. As a particularly elegant demonstration of this capability, a three-dimensional phase envelope was generated for the mixture of sulfur dioxide and nitrogen as presented in the work of Neumann³¹. This phase envelope was first constructed numerically through the use of isotherm tracers, for a range of temperatures from the triple point of sulfur dioxide to the critical point of sulfur dioxide. These isotherms form the skeleton onto which the remaining isolines may be drawn (in three dimensions). In some sense, this is somewhat analogous to construction with *papier-mâché*, the process of which begins with a skeleton formed of chicken wire and wood that is covered with numerous strips of plaster-infused strips of paper. In the phase envelope case, the isobars (analogs of the strips of paper for *papier-mâché*) are drawn around the phase envelope. The starting and ending points of the tracer for the isobars are points on the isolines at the given temperature. Once the isobars and isotherms have been drawn, they are then imported into the `OpenSCAD` package, a script-driven open-source graphical user interface that allows for constructive solid geometry (CSG) operations. The CSG

operations are used to create a solid, three dimensional, object from a set of three dimensional line segments. The CSG output is an STL (STereoLithography) file that can be sent to any 3D printer on the market today.

[Figure 5 about here.]

5.3 Numerical considerations

One of the key challenges when implementing the isochoric thermodynamics formalism to the calculation of phase envelope isolines is that when approaching the critical line, the adaptive integrator can no longer make any progress. This happens because the determinant of the \mathbf{H}_Ψ matrix goes to zero at the critical line. Figure 6 presents results for an isotherm that terminates at the critical point (one of the isolines from Fig. 3b). This figure demonstrates that the adaptive-step-size integrator begins taking small steps (at ρ'_1 near zero), and is able to increase the step size as the integration proceeds. As the critical line is approached, the determinant of \mathbf{H}_Ψ goes to zero, driving the step size to its minimum value, and indicating the presence of the critical point. For this isotherm, the reverse integration is also carried out, and the same phenomenology is also seen; as the integration proceeds, the step size initially increases, and then decreases very rapidly near the critical line, this time from molar concentrations above the values at the critical line.

[Figure 6 about here.]

As an alternative depiction of the progress of the integrator, Fig. 7 shows the molar concentration of the marching variable as a function of step index, for the same tracing as in Fig. 6. At the beginning, step sizes increase, and by about 300 steps, the integrator has reached 99% of its final molar concentration. The remaining steps are in the near-critical region, where the critical behavior drives the determinant of the Hessian matrices to zero, and the step size towards zero as well.

[Figure 7 about here.]

5.4 Computational efficiency results

The key motivator behind this work was reliability of phase equilibrium calculations. Figure 8 shows the results of trying to construct isotherms for a range of temperatures for a mixture of CO₂ and ethane. For all the studied temperatures, the isochoric isotherm tracer succeeds, yielding the curves shown in Fig. 3b. This figure shows the time taken to trace out each of the isotherms; in each case, the molar concentration of the first component is taken as the independent variable, and the integration starts near pure component 2. At low temperatures, far away from the critical line, the isochoric tracer is able to yield the entire isoline from pure fluid to pure fluid in approximately 0.02 seconds. This time includes the polishing steps as well as the time taken to cache variables inside the class.

An alternative implementation is also considered - for each isotherm, 100 molar concentrations, evenly spaced between the molar concentration of near-pure component 2 and the endpoint of the isochoric tracer, are generated. For subcritical

isotherms, this spans from pure fluid to pure fluid, whereas for supercritical isotherms, the values span from the initial values to the values near the critical point. At each molar concentration, the algebraic solver of Eqs. (15) to (17) is used to enforce phase equilibrium. The guess values for the solver are taken from the previous data point. Contrary to the isochoric thermodynamic tracer, a few of the isotherms result in failures at intermediate molar concentrations as is indicated by a missing marker for the algebraic tracer as well as a red "X" marker, failures which in practical application could be quite problematic.

At low temperatures, the isochoric thermodynamics tracer is faster than the algebraic thermodynamics tracer. At higher temperatures, the isochoric thermodynamics solver slows down rapidly because the tracer must asymptotically approach the critical line and take many more than 100 steps. On the other hand, the algebraic solver is "blessed" (in this artificial case) to be able to skip the evaluation of the critical line's location, and can quickly (though less reliably), carry out its calculations. One limitation of the algebraic solver is that it cannot resolve the location of the critical line, a very significant limitation, and one that cannot be appropriately brought out by Fig. 8. The key point is that the algebraic solver, when no knowledge is available about the location of the critical line, will reliably fail for any temperature above the minimum temperature of the critical line. The isochoric isotherm tracer does not have this limitation because it has a built-in brake; the step size decreases smoothly as the tracer approaches the critical line (see for instance Fig. 6).

[Figure 8 about here.]

6 Conclusion

In this work we have described methods that can be used to construct lines of constant pressure and constant temperature cutting through the phase envelope of binary mixtures. These isolines form the conventional p - x and T - x diagrams well known to chemical engineers. The isolines are traced by integrating systems of differential equations along the phase envelope arising from the conditions of phase equilibrium cast into the framework of isochoric thermodynamics. The construction of the isolines is computationally efficient and very reliable. Results are presented in terms of p - x and T - x diagrams, in two and three dimensions. In this work we have focused on simple phase equilibrium isolines; more complex behaviors are possible. Work is ongoing to develop more advanced tracing algorithms able to handle the pitfalls of more complex phase equilibrium behaviors.

Acknowledgments

The authors thank Duncan H. Bell, who generously shared his love of 3D printing and was the inspiration to print a phase envelope in 3D, and Andreas Jäger of TU Dresden for several in-depth reviews of the manuscript.

Literature Cited

- 1 Bell I. H., Jäger A.. Calculation of critical points from Helmholtz-energy-explicit mixture models *Fluid Phase Equilib.* 2017;433:159 – 173.
- 2 Venkatarathnam G.. Density Marching Method for Drawing Phase Envelopes. 3. P-xy Diagrams of Binary Mixtures *Industrial & Engineering Chemistry Research*. 2017;56:13894-13904.
- 3 Deiters U. K.. Differential equations for the calculation of isopleths of multicomponent fluid mixtures *Fluid Phase Equilibria*. 2017;447:72 - 83.
- 4 Quiñones-Cisneros S. E., Deiters U. K.. An efficient algorithm for the calculation of phase envelopes of fluid mixtures *Fluid Phase Equilib.* 2012;329:22-31.
- 5 Michelsen M. L.. Calculation of phase envelopes and critical points for multicomponent mixtures *Fluid Phase Equilib.* 1980;4:1 – 10.
- 6 Deiters U. K., Kraska T.. *High-Pressure Fluid Phase Equilibria: Phenomenology and Computation*. Elsevier 2012.
- 7 Deiters U. K.. Differential equations for the calculation of fluid phase equilibria *Fluid Phase Equilib.* 2016;428:164-173.
- 8 Michelsen M. L., Mollerup J. M.. *Thermodynamic Models: Fundamentals & Computational Aspects*. Tie-Line Publications 2007.
- 9 Castier M.. Helmholtz function-based global phase stability test and its link to the isothermal–isochoric flash problem *Fluid Phase Equilibria*. 2014;379:104 - 111.
- 10 Nichita D. V.. Fast and robust phase stability testing at isothermal–isochoric conditions *Fluid Phase Equilibria*. 2017;447:107 - 124.
- 11 Marquardt D.. An algorithm for least squares estimation of nonlinear parameters *SIAM J. Appl. Math.* 1964;11:431-441.
- 12 Madsen K., Nielsen H. B., Tingleff O.. *Methods for Non-Linear Least Squares Problems* (2nd ed.) 2004.
- 13 Press W. H., Teukolsky S. A., Vetterling W. T., Flannery B. P.. *Numerical Recipes in C*. Cambridge University Press, Cambridge 2002.
- 14 Venkatarathnam G.. Density Marching Method for Calculating Phase Envelopes *Ind. Eng. Chem. Res.* 2014;53:3723-3730.
- 15 Gernert J., Jäger A., Span R.. Calculation of phase equilibria for multi-component mixtures using highly accurate Helmholtz energy equations of state *Fluid Phase Equilib.* 2014;375:209-218.

- 16 Gernert J., Span R.. EOS-CG: A Helmholtz energy mixture model for humid gases and CCS mixtures *J. Chem. Thermodyn.* 2016;93:274–293.
- 17 Kunz O., Klimeck R., Wagner W., Jaeschke M.. *The GERG-2004 Wide-Range Equation of State for Natural Gases and Other Mixtures*. VDI Verlag GmbH 2007.
- 18 Kunz O., Wagner W.. The GERG-2008 Wide-Range Equation of State for Natural Gases and Other Mixtures: An Expansion of GERG-2004 *J. Chem. Eng. Data.* 2012;57:3032-3091.
- 19 Bell I. H., Jäger A.. Helmholtz energy transformations of common cubic equations of state for use with pure fluids and mixtures *J. Res. NIST.* 2016.
- 20 Rowlinson J. S., Swinton F. L.. *Liquids and Liquid Mixtures (Third Edition)*. Butterworth-Heinemann 1982.
- 21 Span R.. *Multiparameter Equations of State - An Accurate Source of Thermodynamic Property Data*. Springer 2000.
- 22 Span R., Wagner W.. A New Equation of State for Carbon Dioxide Covering the Fluid Region from the Triple Point Temperature to 1100 K at Pressures up to 800 MPa *J. Phys. Chem. Ref. Data.* 1996;25:1509-1596.
- 23 Buecker D., Wagner W.. A Reference Equation of State for the Thermodynamic Properties of Ethane for Temperatures from the Melting Line to 675 K and Pressures up to 900 MPa *J. Phys. Chem. Ref. Data.* 2006;35:205-266.
- 24 Span R., Wagner W.. Equations of State for Technical Applications. II. Results for Nonpolar Fluids *Int. J. Thermophys.* 2003;24:41-109.
- 25 Setzmann U., Wagner W.. A New Equation of State and Tables of Thermodynamic Properties for Methane Covering the Range from the Melting Line to 625 K at Pressures up to 1000 MPa *J. Phys. Chem. Ref. Data.* 1991;20:1061-1151.
- 26 Lemmon E. W., McLinden M. O., Wagner W.. Thermodynamic Properties of Propane. III. A Reference Equation of State for Temperatures from the Melting Line to 650 K and Pressures up to 1000 MPa *J. Chem. Eng. Data.* 2009;54:3141-3180.
- 27 Bell I. H., Lemmon E. W.. Automatic Fitting of Binary Interaction Parameters for Multi-fluid Helmholtz-Energy-Explicit Mixture Models *J. Chem. Eng. Data.* 2016;61:3752–3760.
- 28 Wei M. S.-W., Brown T. S., Kidnay A. J., Sloan E. D.. Vapor + Liquid Equilibria for the Ternary System Methane + Ethane + Carbon Dioxide at 230 K and Its Constituent Binaries at Temperatures from 207 to 270 K *J. Chem. Eng. Data.* 1995;40:726-731.
- 29 Brown T. S., Kidnay A. J., Sloan E. D.. Vapor-liquid equilibria in the carbon dioxide-ethane system. *Fluid Phase Equilib.* 1988;40:169-184.

- 30 Jakob W., Rhineland J., Moldovan D.. pybind11 – Seamless operability between C++11 and Python 2016.
<https://github.com/pybind/pybind11>.
- 31 Neumann T.. Development of new Helmholtz Models for Binary Mixtures relevant for CCS Master's Thesis Ruhr-Universität Bochum 2017.

List of Figures

1	p - x diagram for a mixture of CO ₂ + ethane at 230 K with properties calculated from Peng-Robinson mixture model (with $k_{ij} = 0$) and the multi-fluid model. Experimental data (indicated by filled markers for the liquid phase and open markers for the vapor phase) are from the literature ^{28,29}	25
2	Deviation evolution plots as a function composition for two values of the allowable error in the adaptive integrator with and without polishing at each point of the iteration for the 230 K isotherm of an n -hexane + n -octane mixture with ρ'_1 as the marching variable. Lines are shown to guide the eye.	26
3	p - x and T - x diagrams for binary mixtures demonstrating ideal mixing (a), azeotropy with discontinuous isolines at high temperature/pressure (b), and supercritical behavior (c). The critical lines (given by the thick black line) are calculated by the algorithm of Bell and Jäger ¹ . The isotherms and isobars are selected to yield good coverage of the range of validity of the mixture model. The sample code documents what temperatures and pressures were used.	27
4	A screenshot of the <code>plotlyjs</code> -based HTML three-dimensional phase envelope in temperature, pressure and composition for a range of isotherms and isobars for a mixture of CO ₂ + ethane, with properties calculated from the multi-fluid model. An interactive HTML file of this figure is available in the supplemental material.	28
5	A photograph of a three-dimensional phase envelope constructed with the algorithms developed in this work for the mixture of sulfur dioxide and nitrogen, with the multi-fluid model and the mixture model of Neumann ³¹	29
6	Values of the determinant of \mathbf{H}_Ψ and the step size h as a function of the marching variable ρ'_1 for a mixture of CO ₂ + ethane at 300 K with properties calculated from the multi-fluid model	30
7	Marching variable ρ'_1 versus step index for a mixture of CO ₂ + ethane at 300 K with properties calculated from the multi-fluid model	31
8	A speed and reliability test for the isochoric isoline tracer and the algebraic isotherm tracer as a function of the temperature for CO ₂ + ethane, with properties calculated from the multi-fluid model. An “X” marker indicates that the algebraic solver failed although the isochoric tracer was successful. A missing marker indicates that the tracer was unsuccessful.	32

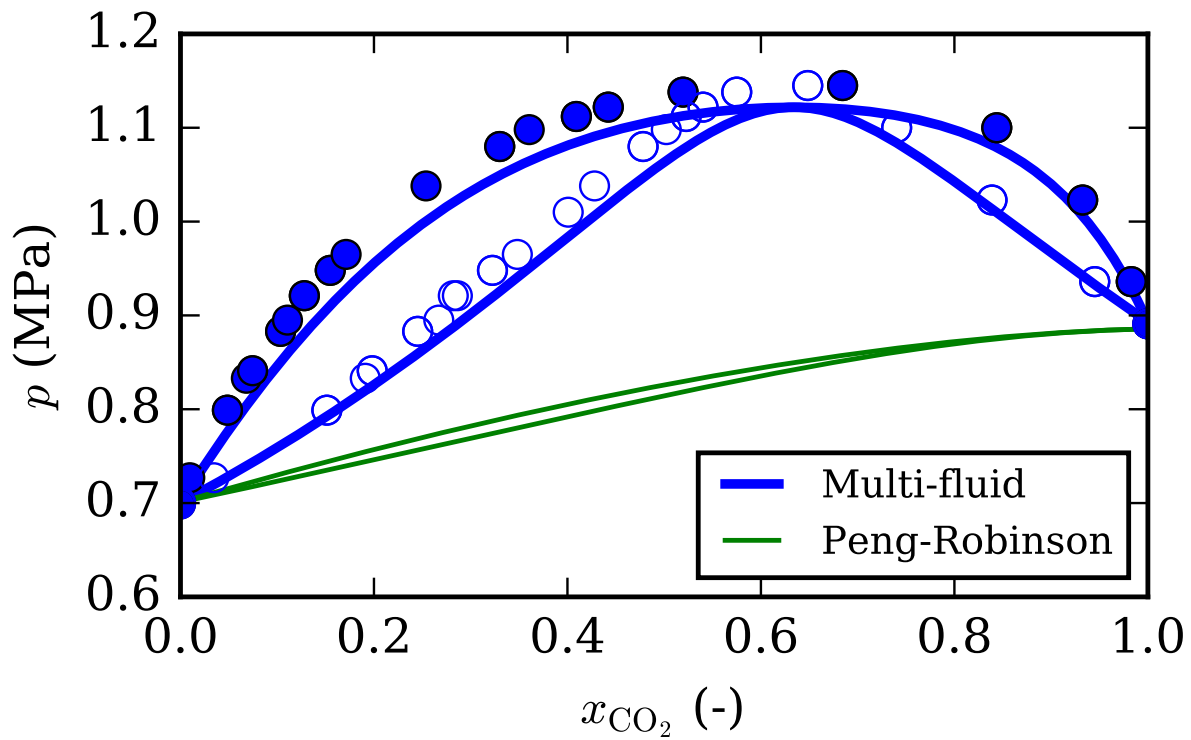
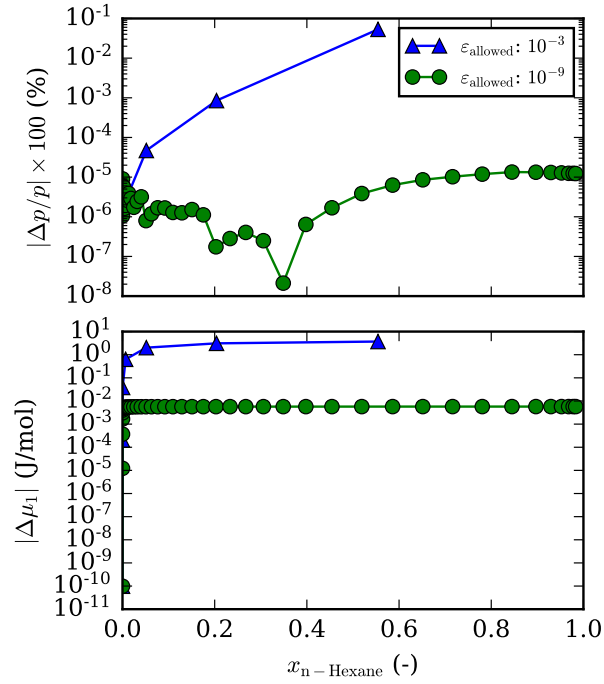
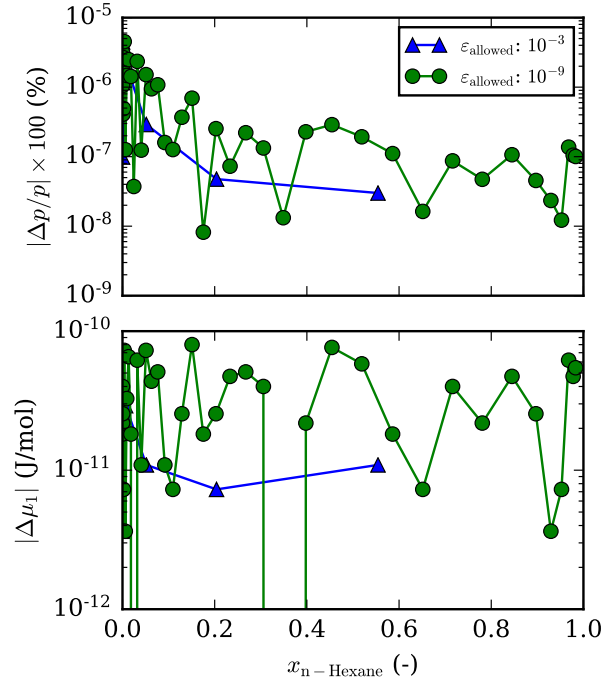


Figure 1: p - x diagram for a mixture of CO_2 + ethane at 230 K with properties calculated from Peng-Robinson mixture model (with $k_{ij} = 0$) and the multi-fluid model. Experimental data (indicated by filled markers for the liquid phase and open markers for the vapor phase) are from the literature^{28,29}.

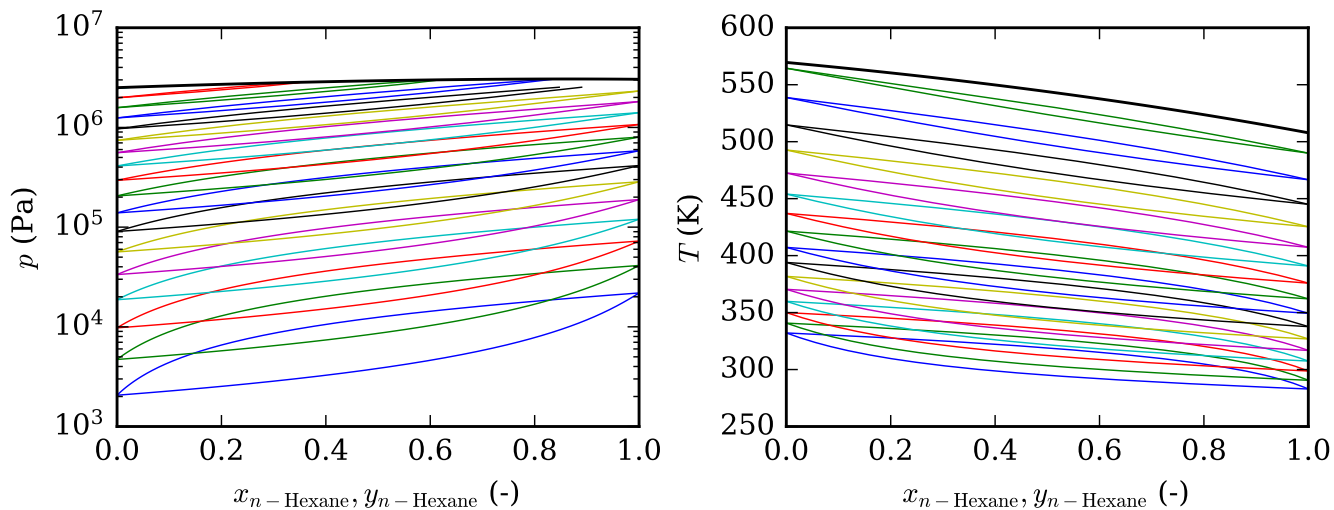


(a) No polishing of the solution during the integration

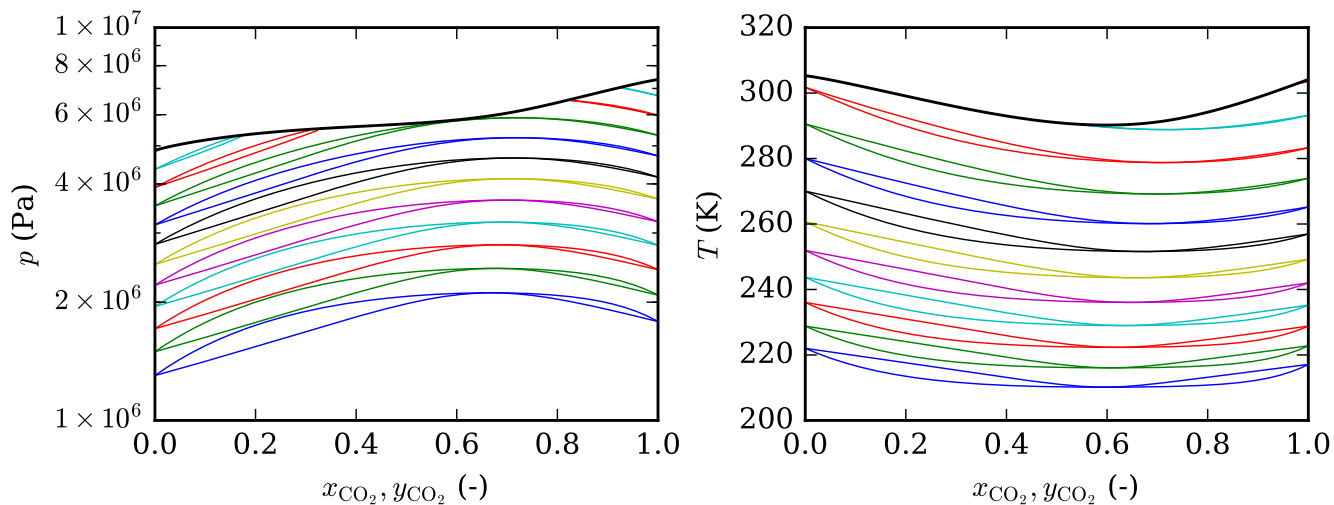


(b) Polishing of the solution at every step

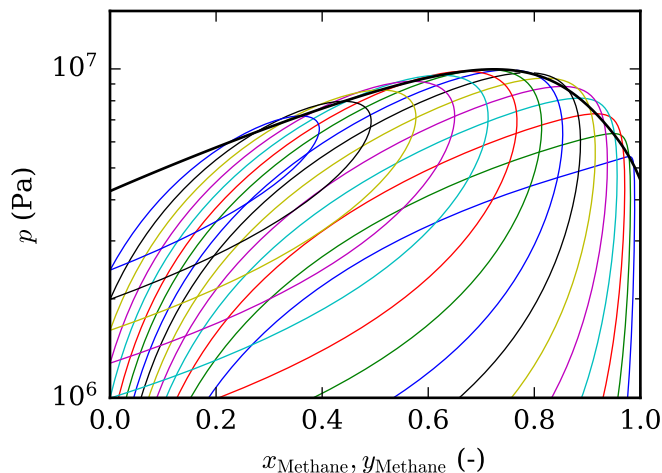
Figure 2: Deviation evolution plots as a function composition for two values of the allowable error in the adaptive integrator with and without polishing at each point of the iteration for the 230 K isotherm of an n -hexane + n -octane mixture with ρ'_1 as the marching variable. Lines are shown to guide the eye.



(a) p - x and T - x diagrams for a mixture of n -hexane + n -octane



(b) p - x and T - x diagrams for a mixture of CO_2 + ethane



(c) p - x diagram for a mixture of methane + n -propane with the Peng-Robinson equation of state (with $k_{ij} = 0$)

Figure 3: p - x and T - x diagrams for binary mixtures demonstrating ideal mixing (a), azeotropy with discontinuous isolines at high temperature/pressure (b), and supercritical behavior (c). The critical lines (given by the thick black line) are calculated by the algorithm of Bell and Jäger¹. The isotherms and isobars are selected to yield good coverage of the range of validity of the mixture model. The sample code documents what temperatures and pressures were used.

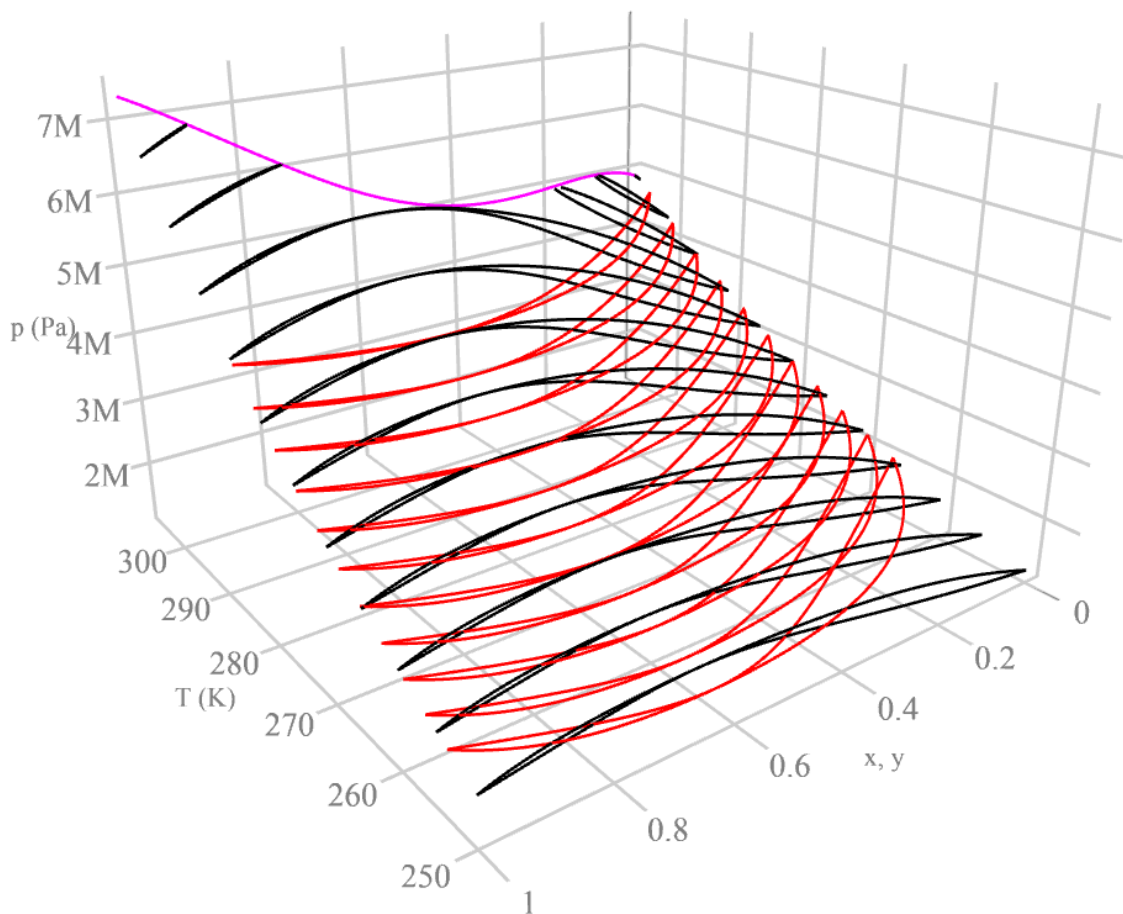


Figure 4: A screenshot of the `plotlyjs`-based HTML three-dimensional phase envelope in temperature, pressure and composition for a range of isotherms and isobars for a mixture of CO₂ + ethane, with properties calculated from the multi-fluid model. An interactive HTML file of this figure is available in the supplemental material.

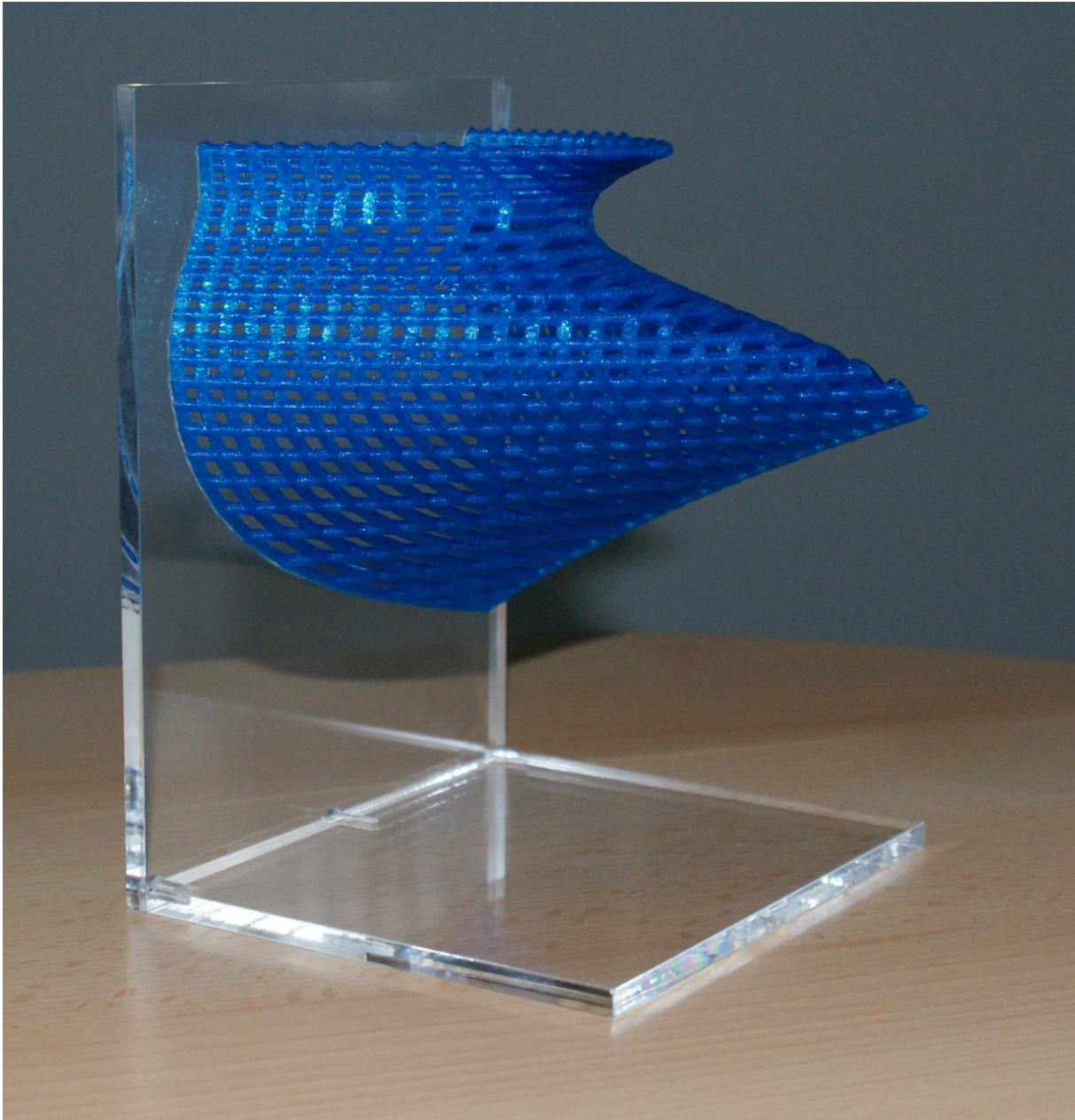


Figure 5: A photograph of a three-dimensional phase envelope constructed with the algorithms developed in this work for the mixture of sulfur dioxide and nitrogen, with the multi-fluid model and the mixture model of Neumann³¹.

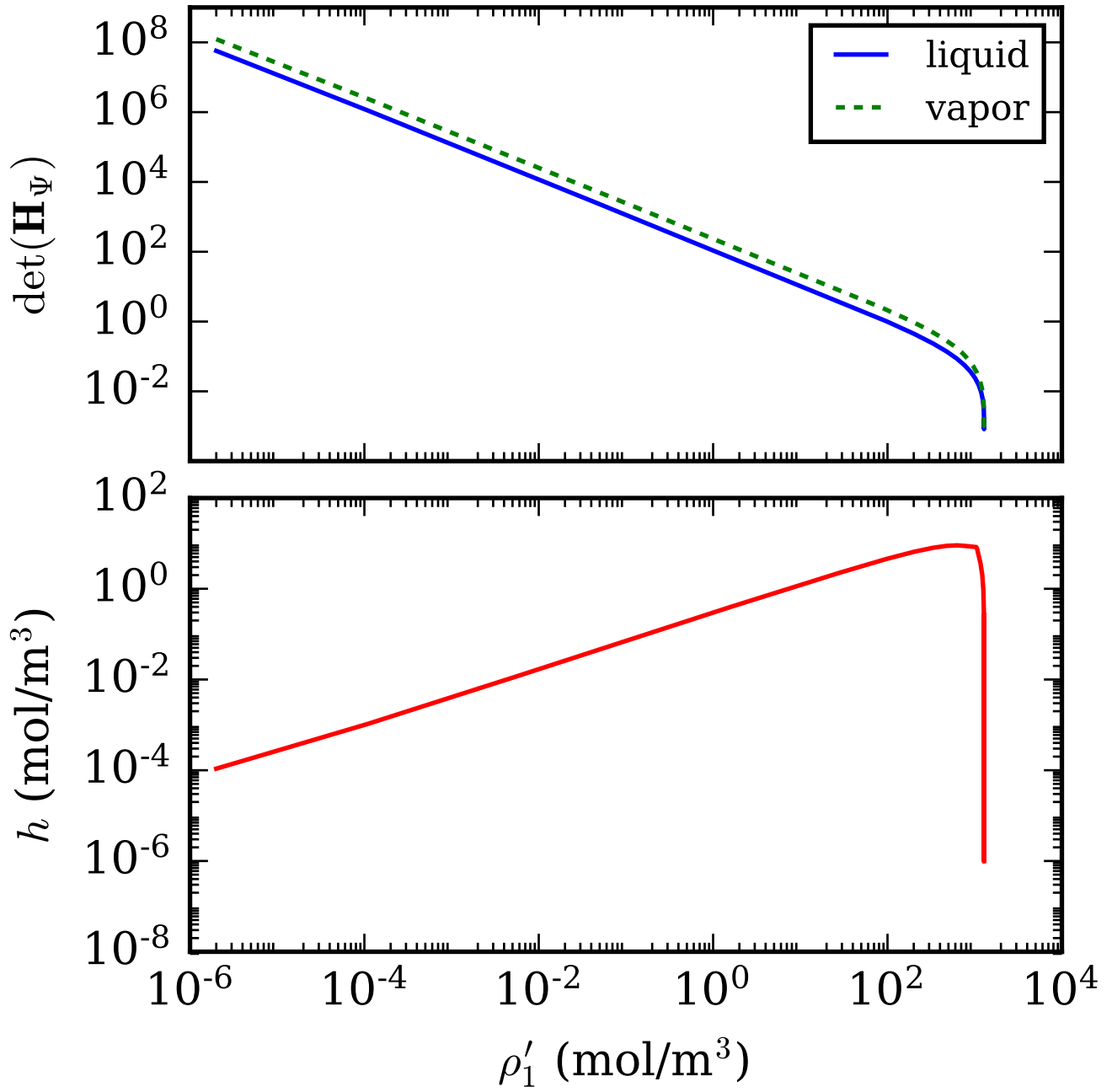


Figure 6: Values of the determinant of \mathbf{H}_Ψ and the step size h as a function of the marching variable ρ_1' for a mixture of CO_2 + ethane at 300 K with properties calculated from the multi-fluid model

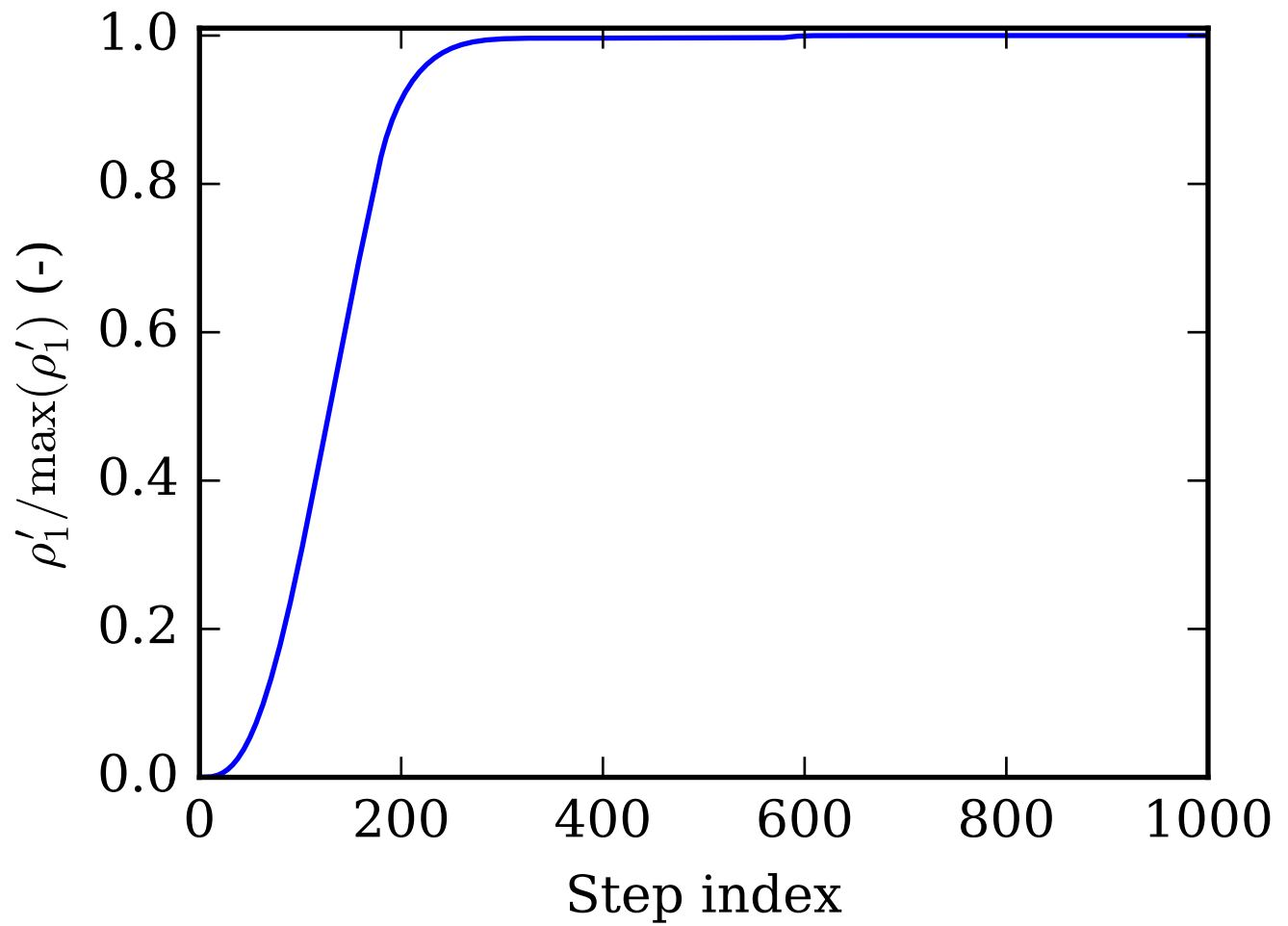


Figure 7: Marching variable ρ'_1 versus step index for a mixture of CO₂ + ethane at 300 K with properties calculated from the multi-fluid model

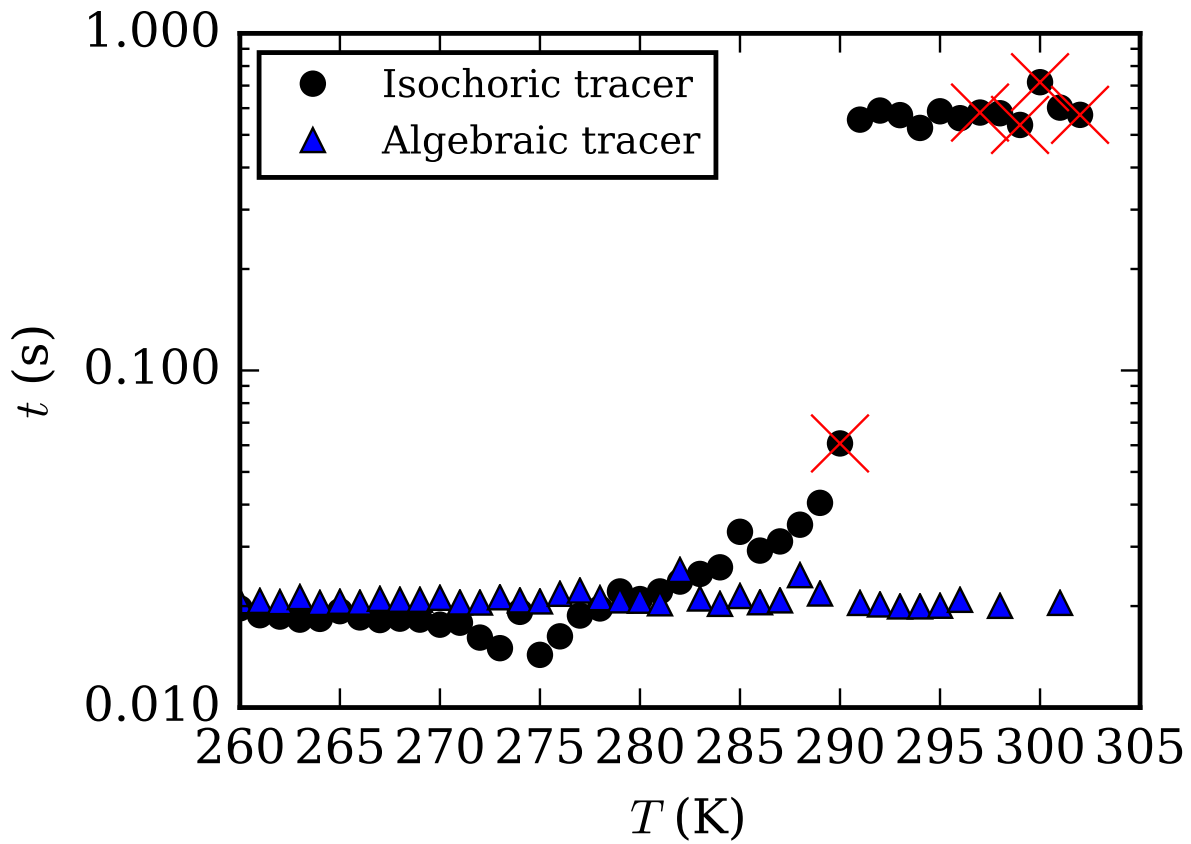


Figure 8: A speed and reliability test for the isochoric isoline tracer and the algebraic isotherm tracer as a function of the temperature for $\text{CO}_2 + \text{ethane}$, with properties calculated from the multi-fluid model. An “X” marker indicates that the algebraic solver failed although the isochoric tracer was successful. A missing marker indicates that the tracer was unsuccessful.

List of Tables

1 Second partial derivatives of Ψ 34

Table 1: Second partial derivatives of Ψ

$$\begin{aligned}
\left(\frac{\partial^2 \Psi}{\partial T \partial \rho_i}\right)_{\rho_j \neq i} &= + \left(\frac{\partial \Psi}{\partial \tau}\right)_{\delta, \vec{x}} \left(\frac{\partial^2 \tau}{\partial T \partial \rho_i}\right)_{T, \rho_j \neq i} \\
&+ \left(\frac{\partial^2 \Psi}{\partial \tau \partial \delta}\right)_{\vec{x}} \left(\frac{\partial \delta}{\partial \rho_i}\right)_{T, \rho_j \neq i} \left(\frac{\partial \tau}{\partial T}\right)_{\vec{\rho}} \\
&+ \left(\frac{\partial^2 \Psi}{\partial \tau^2}\right)_{\delta, \vec{x}} \left(\frac{\partial \tau}{\partial \rho_i}\right)_{T, \rho_j \neq i} \left(\frac{\partial \tau}{\partial T}\right)_{\vec{\rho}} \\
&+ \sum_{m=1}^N \left(\frac{\partial^2 \Psi}{\partial \tau \partial x_m}\right)_{\delta, x_k \neq m} \left(\frac{\partial x_m}{\partial \rho_i}\right)_{T, \rho_j \neq i} \left(\frac{\partial \tau}{\partial T}\right)_{\vec{\rho}}
\end{aligned} \tag{46}$$

$$\begin{aligned}
\left(\frac{\partial^2 \Psi}{\partial \rho_i \partial \rho_j}\right)_T &= \left(\frac{\partial \Psi}{\partial \delta}\right)_{\tau, \vec{x}} \left(\frac{\partial^2 \delta}{\partial \rho_i \partial \rho_j}\right)_T + \left(\frac{\partial \left(\frac{\partial \Psi}{\partial \delta}\right)_{\tau, \vec{x}}}{\partial \rho_j}\right)_{T, \rho_k \neq j} \left(\frac{\partial \delta}{\partial \rho_i}\right)_{T, \rho_j \neq i} \\
&+ \left(\frac{\partial \Psi}{\partial \tau}\right)_{\delta, \vec{x}} \left(\frac{\partial^2 \tau}{\partial \rho_i \partial \rho_j}\right)_T + \left(\frac{\partial \left(\frac{\partial \Psi}{\partial \tau}\right)_{\delta, \vec{x}}}{\partial \rho_j}\right)_{T, \rho_k \neq j} \left(\frac{\partial \tau}{\partial \rho_i}\right)_{T, \rho_j \neq i} \\
&+ \sum_{m=1}^N \left[\left(\frac{\partial \Psi}{\partial x_m}\right)_{\tau, \delta, x_k \neq m} \left(\frac{\partial^2 x_m}{\partial \rho_i \partial \rho_j}\right)_T + \left(\frac{\partial \left(\frac{\partial \Psi}{\partial x_m}\right)_{\tau, \delta, x_k \neq m}}{\partial \rho_j}\right)_{T, \rho_k \neq j} \left(\frac{\partial x_m}{\partial \rho_i}\right)_{T, \rho_j \neq i} \right]
\end{aligned} \tag{47}$$